

3-D Reconstruction of Underwater Object Based on Extended Kalman Filter by Using Acoustic Camera Images

Ngoc Trung Mai*, Hanwool Woo*, Yonghoon Ji*,
Yusuke Tamura*, Atsushi Yamashita*, Hajime Asama*

* Department of Precision Engineering, The University of Tokyo
7-3-1 Hongo, Bunkyo-ku, Tokyo 113-8656, Japan
(e-mail: mai@robot.t.u-tokyo.ac.jp)

Abstract: This paper presents a sensing method to measure three-dimensional (3-D) information in an underwater environment using an acoustic camera. Acoustic cameras can acquire clear information even in turbid water which is difficult to photograph with an optical camera. In addition, its detection range is extensive. Compared to traditional sensors, acoustic cameras with no restrictions on vision are the most powerful sensors for acquiring underwater information. In this paper, we propose a novel approach which enables 3-D measurement of underwater objects using arbitrary viewpoints based on an extended Kalman filter (EKF). By using the probabilistic method based on the EKF, 3-D reconstruction of underwater objects is possible even if the control input for camera movement has uncertainty. Furthermore, since the EKF based estimation is performed sequentially each time, our methodology can be adapted to real-time applications. Simulation and experimental results show the effectiveness of the proposed method.

Keywords: 3-D measurement, underwater sensing, acoustic camera, pose estimation, extended Kalman filter.

1. INTRODUCTION

In recent years, the need of underwater sensing techniques has been increasing. There are numerous tasks in the underwater environment such as inspection, investigation, exploration, etc. (Yoerger et al. (2000)), (Huang et al. (2011)). Until now, many underwater sensing activities still rely on manpower like divers to be carried out. However, in some cases, humans conducting these works directly in underwater environment face many potential dangers. For the dangerous tasks, instead of involving humans directly, exploration by an unmanned robot is desired. Especially, in accidents of nuclear applications, it is necessary to investigate inside in advance for decommissioning tasks. For example, in March 2011, a magnitude 9.0 undersea earthquake occurred off the Pacific coast of Tohoku in east Japan which caused a huge tsunami that destroyed the cooling system of Fukushima Daiichi nuclear power station. This incident has resulted in increased radiation levels inside and outside the plant which brought many problems that need to be solved urgently. However, most of the tasks were very dangerous for humans to carry out. For such cases, robots such as autonomous underwater vehicles (AUVs) and remotely operated underwater vehicles (ROVs) are desired to be applied.

Typically, optical cameras are utilized to obtain information in underwater environments. Since optical cameras

* This work was in part funded by ImPACT Program of Council for Science, Technology and Innovation (Cabinet Office, Government of Japan).

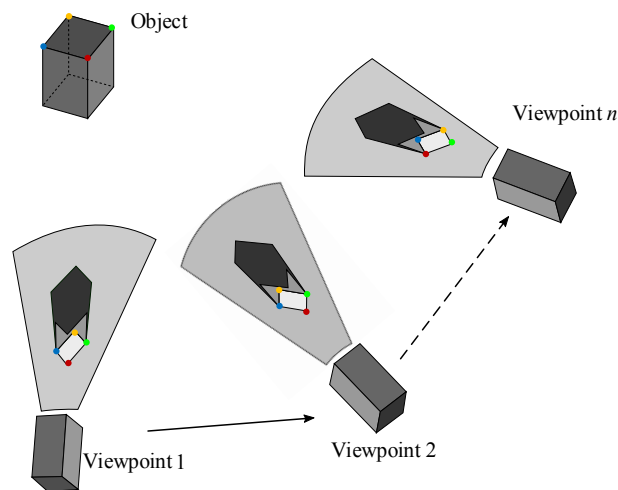


Fig. 1. Observation of an object in a multi-view with an acoustic camera.

have the advantage of obtaining high resolution images, they were used in numerous researches to perform underwater simultaneous localization and mapping (SLAM) (Eustice et al. (2005)), (Eustice et al. (2006)), underwater investigation (Zhang et al. (2011)), and 3-D reconstruction of underwater objects (Pizarro et al. (2004)). However, optical cameras are only suitable for clear water environments and can only be used in very limited areas where light reaches. Under turbid water or light lacking environments, optical cameras cannot be used in general.

On the other hand, ultrasonic sensors can obtain reliable information even in dark or turbid water; thus, they are the most appropriate sensor for underwater sensing. In this respect, measurements for seabed mineral resources, fisheries resources, and seabed topography using ultrasonic sensors have been investigated. More recently, the development of acoustic cameras: dual-frequency identification sonar (DIDSON) and adaptive resolution imaging sonar (ARIS), called next-generation ultrasonic sensor, has enabled the information acquisition in aquatic environments to become more effective (Belcher et al. (2002)). Thanks to the high-resolution acoustic images of acoustic cameras, a number of methodologies using acoustic camera-based systems have been proposed for sensing the underwater environment, such as mosaicing (Hurtos et al. (2014)), underwater object detections (Cho et al. (2015)), and location estimation of AUVs (Johannsson et al. (2010)).

Furthermore, other researches have proposed methods for system calibration and 3-D scene construction by applying opti-acoustic fusion system (Negahdaripour et al. (2009)), (Babae and Negahdaripour (2013)). These studies have improved the accuracy of the 3-D measurement of underwater objects by applying opti-acoustic stereo imaging system calibration which is composed of one sonar and one optical camera. However, this system still relies on optical vision, which will reduce its range in turbid water. Other than that, 3-D measurement techniques for underwater objects using the acoustic camera images on a multi-view have also been proposed by Aykin et al. (Aykin and Negahdaripour (2015)), Kwak et al. (Kwak et al. (2016)), and Ji et al. (Ji et al. (2016)). All of these studies strictly assumed that the exact pose (i.e., position and orientation) of the acoustic camera in multi-views is known before carrying out the 3-D measurement of underwater objects. However, especially in underwater environments, it is difficult to accurately grasp the pose information of the acoustic camera, so it is inevitable that errors occur in the movement control information of the acoustic camera. As a result, the accuracy of 3-D measurement deteriorates. Therefore, in order to perform a more accurate 3-D measurement, it is necessary to consider the pose errors for the movement of the acoustic camera. A novel algorithm for recovery of 3-D feature points using acoustic images from multi-view while also constraining the poses from which the images are taken has been proposed by Huang et al. (Huang and Kaess (2015)). They recovered 3-D feature points based on an optimization approach for the Bayesian SLAM. However, the method used in this research required to collect all of the data of measurement and movement of the camera before performing the optimization. Thus, it cannot be used in real-time applications, which are necessary for the case of unmanned exploration tasks.

The contributions of this paper are as follows. Previous approaches in which the pose error of each viewpoint could not be considered have a significant limitation on the 3-D measurement accuracy, as mentioned above. Moreover, we should implement not the offline algorithm but the online algorithm for the real-time application. Therefore, the proposed 3-D measurement scheme in this paper is able to manage the pose errors of the acoustic camera as well as the online process. Figure 1 illustrates a conceptual image of the proposed method based on multiple acoustic views.

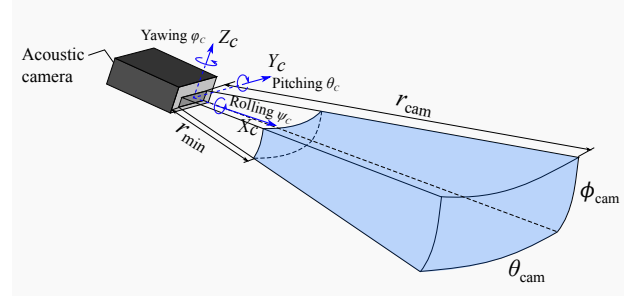


Fig. 2. Geometrical model in the acoustic camera image generation.

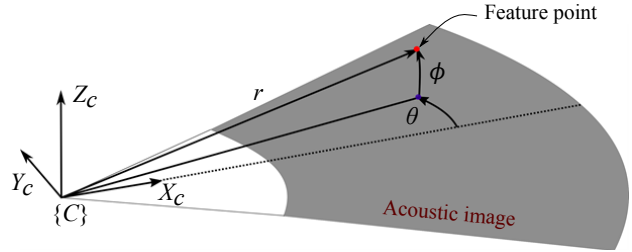


Fig. 3. Imaging sonar geometry. The values of the range r and azimuth angle θ can be obtained from the pixel coordinate of acoustic image, while the elevation angle ϕ is missing.

In order to measure the 3-D position of the feature points of the underwater object while estimating the accurate poses of the acoustic camera, we use an extended Kalman filter (EKF)-based approach. The estimation of the 3-D position of the feature points and the latest pose of the camera is sequentially performed at each time. Thus, our novel method can be used in real-time applications.

2. PRELIMINARIES OF ACOUSTIC CAMERA

2.1 Acoustic projection model

An acoustic camera generates an acoustic image by transmitting ultrasonic waves in a 3-D area space. Its sensing range is determined by the maximum measuring range r_{cam} , minimum measuring range r_{min} , azimuth angle θ_{cam} , and elevation angle ϕ_{cam} , as shown in Fig. 2. The ultrasonic waves propagate forward, hit the underwater object and are reflected. The acoustic camera receives reflected waves from the object, then calculates the power of the reflected waves, and reports it at the pixel corresponding to the direction of the reflected waves on a power map.

2.2 Imaging acoustic geometry

Although an acoustic camera senses a 3-D area, the output of the sensing process is a 2-D acoustic image. As shown in Fig. 3, the acoustic image provides the range r and the azimuth angle θ , while the elevation angle ϕ is missing. Therefore, it is generally impossible to take the 3-D information of objects by using a single acoustic image. To solve this problem, a theoretical methodology to recover 3-D coordinates by using multi-acoustic images from different viewpoints is proposed and will be discussed in the next section.

3. EKF-BASED 3-D MEASUREMENT METHODOLOGY

3.1 Problem setting

An overview of the proposed method in this study is shown in Fig. 4. For the input information, sequential images from the acoustic camera and control input data for camera movements are used. The 3-D positions of feature points which are the bare bones of the underwater objects and the 6-degrees of freedom (DOF) acoustic camera poses are estimated from an EKF algorithm as the output information. State vectors, that indicate the camera pose \mathbf{x}_c and the positions of feature points $\mathbf{x}_l(1:n)$, are defined as follows:

$$\mathbf{x}_c = [x_c \ y_c \ z_c \ \psi_c \ \theta_c \ \varphi_c]^\top, \quad (1)$$

$$\mathbf{x}_l(1:n) = [\mathbf{x}_{l1}^\top \ \mathbf{x}_{l2}^\top \ \dots \ \mathbf{x}_{ln}^\top]^\top, \quad (2)$$

$$\mathbf{x}_{li} = [x_{li} \ y_{li} \ z_{li}]^\top. \quad (3)$$

Next, \mathbf{X} is defined as the system state vector, whose elements are \mathbf{x}_c and $\mathbf{x}_l(1:n)$, as follows:

$$\mathbf{X} = [\mathbf{x}_c^\top \ \mathbf{x}_l(1:n)^\top]^\top. \quad (4)$$

Here, \mathbf{P} is also defined as the covariance matrix, indicating the uncertainty of the state vector \mathbf{X} , as follows:

$$\mathbf{P} = \begin{bmatrix} \mathbf{P}_c & \mathbf{P}_{c,l} \\ \mathbf{P}_{l,c} & \mathbf{P}_l \end{bmatrix}, \quad (5)$$

where the diagonal elements \mathbf{P}_c and \mathbf{P}_l are covariance matrices corresponding to the state vector of the camera pose and feature points, respectively. The off-diagonal element $\mathbf{P}_{l,c} = \mathbf{P}_{c,l}$ is the cross-correlation matrices of \mathbf{P}_c and \mathbf{P}_l . The EKF-based estimation procedure consists of a prediction and an update step. First, in the prediction step, the system state \mathbf{X} and corresponding covariance \mathbf{P} are predicted based on the control input data for the camera movement. Next, in the update step, the system state \mathbf{X} and corresponding covariance \mathbf{P} are updated based on the measurement data.

3.2 Movement model and prediction step

In the prediction step, the state vector \mathbf{X}_t and corresponding covariance matrix \mathbf{P}_t at time t are predicted as follows:

$$\bar{\mathbf{X}}_t = \mathbf{g}(\mathbf{u}_t, \mathbf{X}_{t-1}), \quad (6)$$

$$\bar{\mathbf{P}}_t = \mathbf{G}_t \mathbf{P}_{t-1} \mathbf{G}_t^\top + \mathbf{R}_t. \quad (7)$$

Here, function $\mathbf{g}(\cdot)$ represents a movement model function of the system, \mathbf{R}_t is the process noise, and $\mathbf{G}_t = \partial \mathbf{g} / \partial \mathbf{X}_{t-1}$ is the Jacobian matrix of the motion model. When applying the control input \mathbf{u}_t of the camera movement, the state vector \mathbf{X}_t and corresponding covariance \mathbf{P}_t at time t are predicted based on \mathbf{X}_{t-1} and \mathbf{P}_{t-1} by (6) and (7). In this way, in the prediction step, using the control input data for the camera movement and the process noise to predict the state vector and covariance matrix. In this step, measurement information from the acoustic images is still yet to be reflected.

3.3 Measurement model and update step

In the update step, the measurement information from the acoustic images is used to update the state vector \mathbf{X}_t

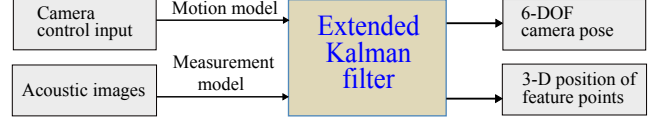


Fig. 4. Overview of the proposed method. Extended Kalman filter algorithm is used to estimate the camera pose and the positions of feature points.

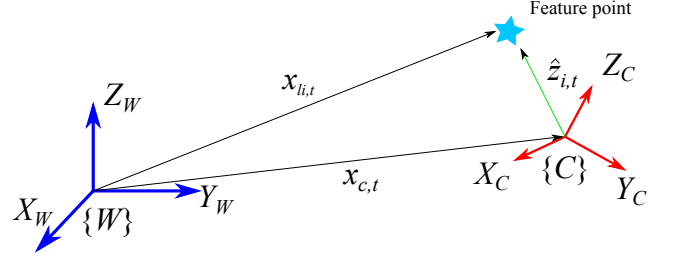


Fig. 5. Overview of measurement model. (X_w, Y_w, Z_w) is world coordinate system and (X_c, Y_c, Z_c) is camera coordinate system.

and covariance matrix \mathbf{P}_t . In this study, the measurement information is defined as feature points on the acoustic image. The feature points indicate vertices of objects whose reflection intensity changes suddenly, that make acoustic pressure values change rapidly in the acoustic image. In this step, firstly, for each measurement, the expected measured value is calculated. The expected measured value can be estimated by a state vector as follows:

$$\hat{\mathbf{z}}_t = \mathbf{h}(\bar{\mathbf{X}}_t). \quad (8)$$

Here, it is necessary to define a measurement model $\mathbf{h}(\cdot)$ for the feature points of the underwater objects. As shown in Fig. 5, besides the world coordinate system (X_w, Y_w, Z_w) , the camera coordinate system (X_c, Y_c, Z_c) is also defined. From the position information of the feature point $(x_{li,t}, y_{li,t}, z_{li,t})$ in the world coordinate system, the position of the feature point $(x'_{li,t}, y'_{li,t}, z'_{li,t})$ in the camera coordinate system is obtained as follows:

$$\begin{bmatrix} x'_{li,t} \\ y'_{li,t} \\ z'_{li,t} \end{bmatrix} = \mathbf{R}_t \begin{bmatrix} x_{li,t} - x_{c,t} \\ y_{li,t} - y_{c,t} \\ z_{li,t} - z_{c,t} \end{bmatrix}, \quad (9)$$

where $(x_{c,t}, y_{c,t}, z_{c,t})$ is the position of the camera, and \mathbf{R}_t is the rotation matrix of the coordinate transformation. For the acoustic camera, the measurement information $\hat{\mathbf{z}}_t$ consists of the distance \hat{r} and azimuth angle $\hat{\theta}$ which can be obtained by following equation.

$$\hat{\mathbf{z}}_{i,t} = \begin{bmatrix} \hat{r}_{i,t} \\ \hat{\theta}_{i,t} \end{bmatrix} = \begin{bmatrix} \sqrt{x'^2_{li,t} + y'^2_{li,t} + z'^2_{li,t}} \\ \tan^{-1}(y'_{li,t} / x'_{li,t}) \end{bmatrix}. \quad (10)$$

Next, the Kalman gain \mathbf{K}_t is calculated from the actually measured measurement information \mathbf{z}_t and predicted $\hat{\mathbf{z}}_t$ as follows:

$$\mathbf{K}_t = \bar{\mathbf{P}}_t \mathbf{H}_t^\top (\mathbf{H}_t \bar{\mathbf{P}}_t \mathbf{H}_t^\top + \mathbf{Q}_t)^{-1}. \quad (11)$$

Then, using the Kalman gain \mathbf{K}_t , the state vector \mathbf{X}_t and the covariance matrix \mathbf{P}_t are updated as the following equations.

$$\mathbf{X}_t = \bar{\mathbf{X}}_t + \mathbf{K}_t(\mathbf{z}_t - \hat{\mathbf{z}}_t), \quad (12)$$

$$\mathbf{P}_t = (\mathbf{I} - \mathbf{K}_t \mathbf{H}_t) \bar{\mathbf{P}}_t, \quad (13)$$

where \mathbf{Q}_t is the noise matrix on the measurement value, and \mathbf{H}_t is the Jacobian matrix of the measurement model.

4. EXPERIMENTAL RESULTS

In order to verify the proposed methodologies, simulation and real experiments were conducted. The proposed method introduced in Section 3 was applied to measure the 3-D information of underwater objects.

4.1 Simulation

In the simulation experiment, we assumed that all feature points and their corresponding relationships are known. We used a square prism as the underwater object. Its multiple vertices allow us to extract a plurality of feature points. The number of feature points was $n=8$, and the number of viewpoints was $T=21$. The error of the movement control was assumed to follow a normal distribution, and set proportional to the moving amount. In this experiment, the object was fixed and ahead about 2.5 m from the initial position of the acoustic camera. The trajectory of the camera was set to always face the direction of the object. In the 6-DOF of the camera pose $(x_c, y_c, z_c, \psi_c, \theta_c, \varphi_c)$, (x_c, y_c, z_c) represents the 3-D camera position and $(\psi_c, \theta_c, \varphi_c)$ represents the camera orientation. Of all the trajectory sets of the camera, the values of x_c, y_c, z_c, ψ_c fluctuated, meanwhile the values of θ_c and φ_c were always 0. As initial set of feature points, we used the first measured information of each feature point, consisting of the distance r and azimuth angle θ . The initial values of the unknown elevation angles ϕ were set to 0. The relative position of the camera trajectory and the target object is shown in Fig. 6.

The errors of the camera pose estimated by the proposed method and odometry (i.e., only using the motion model, (6)) are shown in Fig. 7. Figure 7(a) shows the error of the estimated camera position. As shown in Fig. 7(a), the error in the odometry accumulates and tends to be large. However, the error of the estimated camera position which was obtained using the proposed method is kept within a certain range. Similarly, the error of the estimated camera orientation ψ_c is shown in Fig. 7(b). The similar tendency as in Fig. 7(a) can also be seen in Fig. 7(b).

The estimation results of the 3-D information of the feature points are shown in Fig. 8(a). The blue and green dots represent the initial values and the true values of each feature point respectively. The red dots represent the estimated values of each feature point. As shown in Fig. 8(a), the estimated points are much closer to the true values although the initial points were set far from the true values. The relationship between the number of observations and its estimated error is shown in Fig. 8(b). In the initial setting, the error of each feature point was about 0.2 m for feature points (P, Q, R, S) and about 0.3 m for feature points (T, U, V, W). As the number of observations increases, these errors tend to decrease gradually and be approximately 0.008–0.012 m at the end of the estimation results.

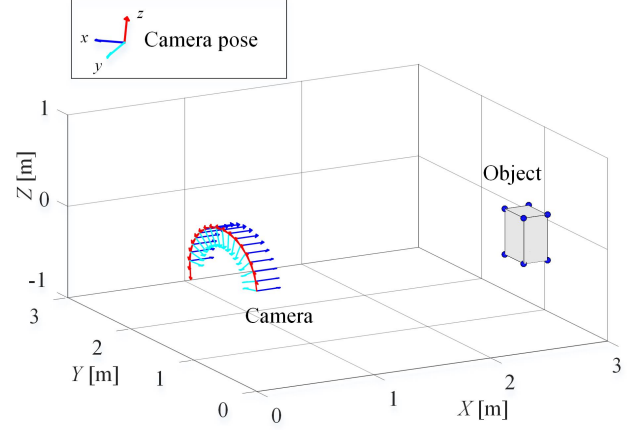


Fig. 6. The relative position of the camera and the object. A square prism was used as the underwater object and the camera was set to always face the direction of the object.

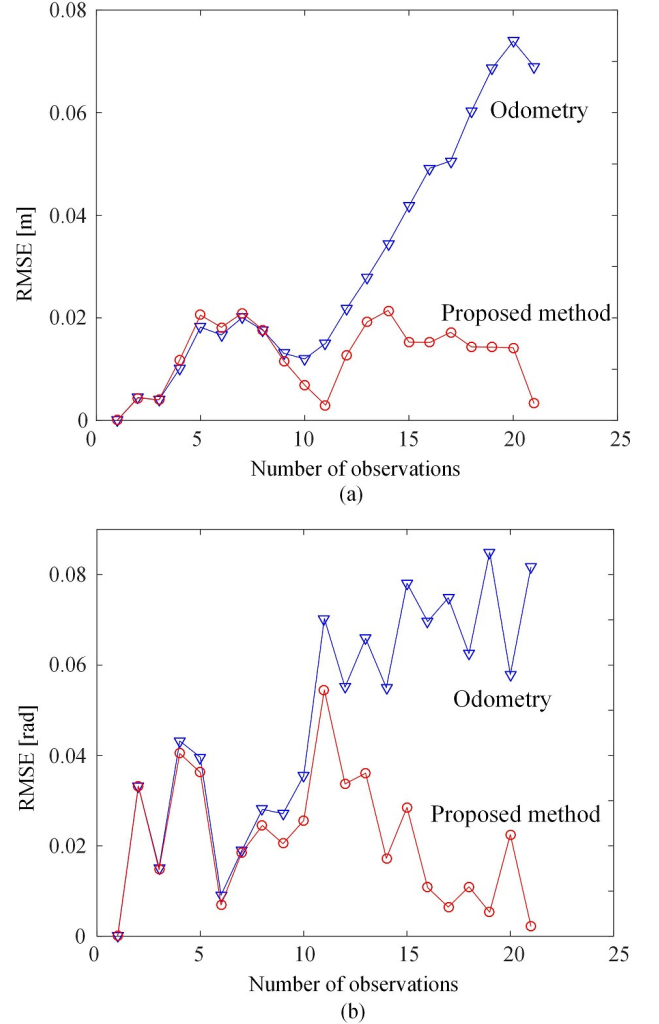


Fig. 7. The errors of the camera pose estimated by the proposed method and odometry: (a) the error of the estimated camera position and (b) the error of the estimated camera orientation ψ_c .

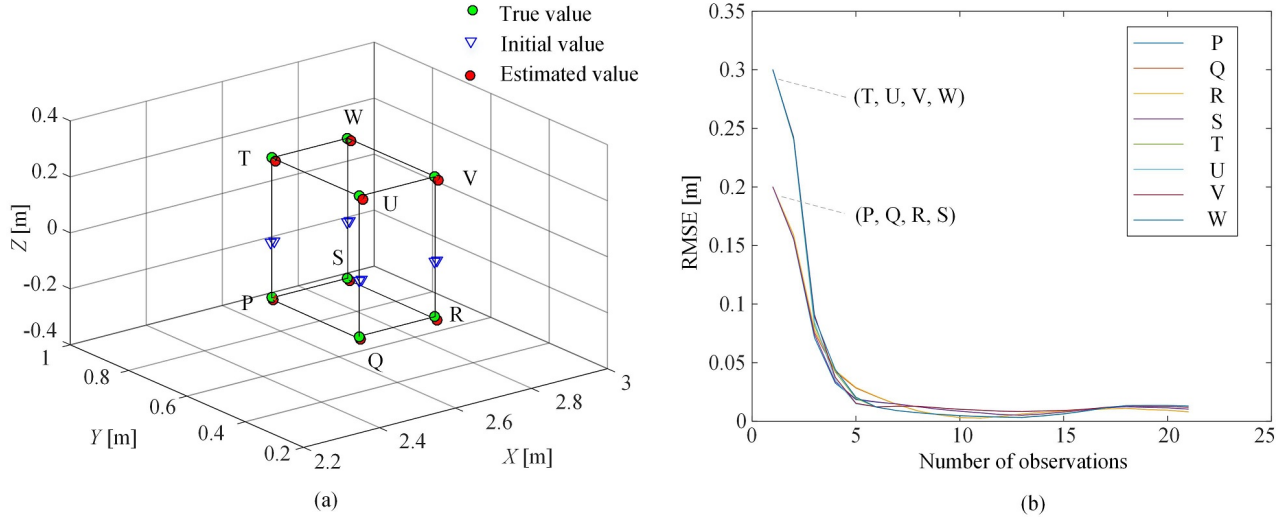


Fig. 8. Experimental results for 3-D reconstruction of the square prism: (a) the 3-D positions of 8 vertices of the square prism were measured by proposed method. The green dots indicate the ground truth, the blue triangle marks indicate the initial set values, and the red dots indicate the estimated values and (b) the relationship between the number of observations and the error of the estimated feature points.

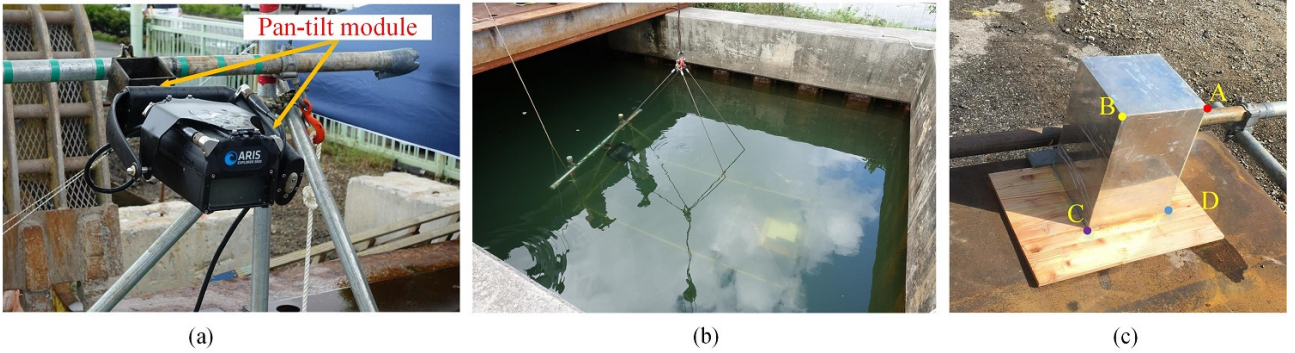


Fig. 9. The acoustic camera and underwater object were used in the real experiment: (a) the acoustic camera (ARIS EXPLORER 3000) with the pan-tilt module, (b) the experimental environment in turbid tank, and (c) the underwater object.

4.2 Real experiment

In this subsection, the results of real experiments will be discussed in order to verify the validity of the proposed methodologies. The experiment was conducted using ARIS EXPLORER 3000, as shown in Fig. 9(a). Its detailed specifications are shown in Table 1. In addition, this experiment was conducted in a turbid tank, as shown in Fig. 9(b). We utilized a square prism (200W 200L 300H mm) as the underwater object, as shown in Fig. 9(c). The experimental conditions were close to the conditions of the simulation introduced in Subsection 4. 1. The experimental system with the acoustic camera and square prism was set up and brought under water, about 4 m from the water surface. The square prism was set ahead about 2.5 m from the initial position of the acoustic camera. The acoustic camera was located higher than the objects to insonify acoustic waves at the objects diagonally. As shown in Fig. 9(a), the acoustic camera was tilted down about 20 deg.

From this experiment, a number of acoustic images were acquired at different acoustic camera poses, especially

Table 1. Specifications of ARIS EXPLORER 3000

Identification frequency	3 MHz
Detection frequency	1.8 MHz
Depth Rating	300 m
Identification range r_{cam}	5 m
Azimuth angle θ_{cam}	32 deg
Elevation angle ϕ_{cam}	14 deg
Number of transducer beams	128
Beam width	0.25 deg

rolling ψ_c of the acoustic camera. We defined the world coordinate with reference to the initial camera pose. In other words, the 6-DOF of the initial camera pose was (0, 0, 0, 0, 0, 0). The following camera poses were transformed by rolling by 10 deg from 0 deg to 70 deg. The control input data for the rolling were obtained from pan-tilt module as shown in Fig. 9(a).

The acoustic images of the object utilized in 3-D measurement are shown in Fig. 10. Even in turbid water, the acoustic camera was capable of providing the information of the object. Four vertices of the square prism, which were labelled as A, B, C, and D as shown in Fig. 9(c), were

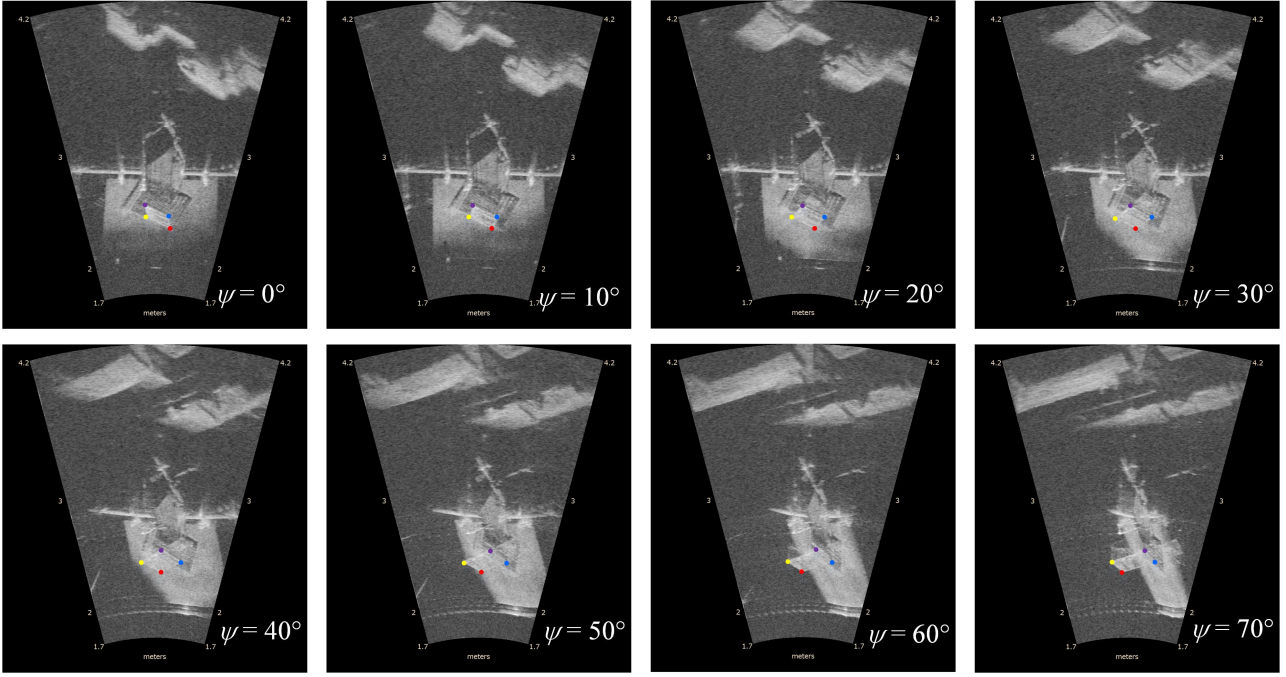


Fig. 10. The real acoustic images of the square prism with different camera poses.

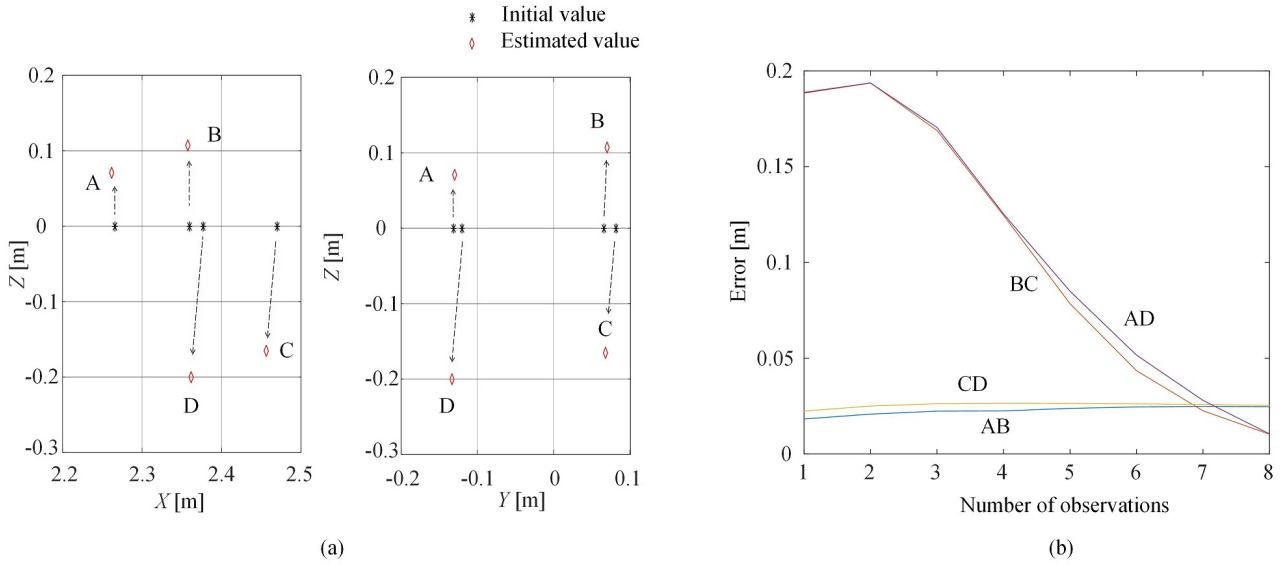


Fig. 11. The results of the real experiment: (a) the estimated result of the feature points in the real experiment and (b) the errors of the edges of the rectangle.

manually selected as the corresponding feature points in the acoustic images, as shown in Fig. 10. In the first camera pose, where $\psi_c = 0$, points A and B of the square prism were closer to the acoustic camera position than points C and D. Thus, in the first acoustic image, points A and B were mapped into pixels that correspond with a smaller range, as shown in left top of Fig. 10. The movement of the feature points in the real acoustic images corresponding to the motion of the acoustic camera (i.e., $\psi_c = 0-70$ deg) can be seen from Fig. 10.

Figure 11 presents the results of the measured 3-D feature points of the object. For the initial set of the feature points, the values of the unknown elevation angles ϕ were set to 0.

Thus, the values of initial z of all feature points were 0. As the number of observations increases, the estimated z moves down or up as shown in Fig. 11(a). Moreover, the errors of the lengths of the edges AD and BC tend to decrease, as shown in Fig. 11(b). Note that the values of x and y of the feature points did not change much between the initial setting and the final estimated result as shown in Fig. 11(a), meanwhile the values of z changed very much.

In the real experiment, as shown in Fig. 9(c), feature points (A, B) and (C, D) have almost the same height z , respectively. Thus, when we set the initial values z of feature points A, B, C, and D same to 0, the lengths of the edges AB and CD were already close to true values

from the beginning; therefore, the errors of the lengths of the edges AB and CD were already small from the beginning and had not tended to decrease, as shown in Fig. 11(b). Meanwhile, the errors of the edges AD and BC were reduced significantly. In the initial setting, errors of the edges AD and BC were about 0.18 m. These errors decreased gradually and were approximately 0.01 m at the end of the estimation results.

Consequently, both of the simulation and real experimental results showed that the proposed methodologies are effective for the 3-D measurement of underwater objects.

5. CONCLUSION

In this study, we proposed a novel methodology to get the 3-D information of the feature points of underwater object based on the EKF using acoustic camera images in multi-view. By using the probabilistic method based on the EKF, even though there is uncertainty in the control input camera, 3-D reconstruction of underwater object is available. Moreover, since the EKF estimation is sequentially performed at each time, our novel methodology can be used in real-time applications. Experiments were performed in both simulation and real environments in order to demonstrate the effectiveness of the proposed method.

In the future, the automatic extraction and correspondences of features will be addressed. In this study, the feature point was handled, which is a low-level feature. In our next work, high-level features such as lines and plane, which are suitable for acoustic camera images for automatic extraction and automatic association of the features, will be considered.

ACKNOWLEDGEMENTS

The authors would like to thank S. Fuchiyama, A. Ueyama, and their colleagues at KYOKUTO Construction Co., Ltd. for full access to their facilities for the real experiment. We would also like to thank Y. Yamamura, F. Maeda, and S. Imanaga at TOYO Corp. who helped in this research project over a day for the equipment set up and the acquisition of the sonar data.

REFERENCES

- Aykin, M.D. and Negahdaripour, S. (2015). On 3-D Target Reconstruction from Multiple 2-D Forward-Scan Sonar Views. In *Proceedings of the 2015 MTS/IEEE OCEANS Conference and Exhibition*, 1–10. IEEE.
- Babaee, M. and Negahdaripour, S. (2013). 3-D Object Modeling From Occluding Contours in Opti-Acoustic Atereo Images. In *Proceedings of the 2013 MTS/IEEE OCEANS Conference and Exhibition*, 1–8. IEEE.
- Belcher, E., Hanot, W., and Burch, J. (2002). Dual-Frequency Identification Sonar (DIDSON). In *Proceedings of the 2002 International Symposium on Underwater Technology*, 187–192. IEEE.
- Cho, H., Gu, J., Joe, H., Asada, A., and Yu, S.C. (2015). Acoustic Beam Profile-Based Rapid Underwater Object Detection for an Imaging Sonar. *Journal of Marine Science and Technology*, volume 20(1), 180–197.
- Eustice, R., Singh, H., Leonard, J.J., Walter, M.R., and Ballard, R. (2005). Visually Navigating the RMS Titanic with SLAM Information Filters. In *Proceedings of the Robotics: Science and Systems*, volume 2005, 57–64.
- Eustice, R.M., Singh, H., Leonard, J.J., and Walter, M.R. (2006). Visually Mapping the RMS Titanic: Conservative Covariance Estimates for SLAM Information Filters. *The International Journal of Robotics Research*, volume 25(12), 1223–1242.
- Huang, T.A. and Kaess, M. (2015). Towards Acoustic Structure from Motion for Imaging Sonar. In *Proceedings of the 2015 International Conference on Intelligent Robots and Systems (IROS)*, 758–765. IEEE.
- Huang, Y.W., Sasaki, Y., Harakawa, Y., Fukushima, E.F., and Hirose, S. (2011). Operation of Underwater Rescue Robot Anchor Diver III During the 2011 Tohoku Earthquake and Tsunami. In *Proceedings of the 2011 MTS/IEEE OCEANS*, 1–6. IEEE.
- Hurtos, N., Nagappa, S., Palomeras, N., and Salvi, J. (2014). Real-Time Mosaicing with Two-Dimensional Forward-Looking Sonar. In *Proceedings of the 2014 International Conference on Robotics and Automation (ICRA)*, 601–606. IEEE.
- Ji, Y., Kwak, S., Yamashita, A., and Asama, H. (2016). Acoustic Camera-based 3-D Measurement of Underwater Objects through Automated Extraction and Association of Feature Points. In *Proceedings of the 2016 International Conference on Multisensor Fusion and Integration for Intelligent Systems (MFI)*, 224–230. IEEE.
- Johannsson, H., Kaess, M., Englot, B., Hover, F., and Leonard, J. (2010). Imaging sonar-aided navigation for autonomous underwater harbor surveillance. In *Proceedings of the 2010 International Conference on Intelligent Robots and Systems (IROS)*, 4396–4403. IEEE.
- Kwak, S., Ji, Y., Yamashita, A., and Asama, H. (2016). 3-D Reconstruction of Underwater Objects Using Arbitrary Acoustic Views. In *Proceedings of the 11th France-Japan congress on Mechatronics / the 9th Europe-Asia congress on Mechatronics / the 17th International Conference on Research and Education in Mechatronics (MECATRONICS-REM2016)*, 74–79. IEEE.
- Negahdaripour, S., Sekkati, H., and Pirsiavash, H. (2009). Opti-Acoustic Stereo Imaging: On System Calibration and 3-D Target Reconstruction. *IEEE Transactions on Image Processing*, volume 18(6), 1203–1214.
- Pizarro, O., Eustice, R., and Singh, H. (2004). Large Area 3-D Reconstructions from Underwater Surveys. In *Proceedings of the 2004 MTS/IEEE OCEANS Conference and Exhibition*, volume 2, 678–687. IEEE.
- Yoerger, D.R., Bradley, A.M., Walden, B.B., Cormier, M.H., and Ryan, W.B. (2000). Fine-Scale Seafloor Survey in Rugged Deep-Ocean Terrain with an Autonomous Robot. In *Proceedings of the 2000 International Conference on Robotics and Automation (ICRA)*, volume 2, 1787–1792. IEEE.
- Zhang, Y., McEwen, R.S., Ryan, J.P., Bellingham, J.G., Thomas, H., Thompson, C.H., and Rienecker, E. (2011). A peak-Capture Algorithm Used on an Autonomous Underwater Vehicle in the 2010 Gulf of Mexico Oil Spill Response Scientific Survey. *Journal of Field Robotics*, volume 28(4), 484–496.